

Article

Oxidative Cleavage of 9,10-Dihydroxystearic Acid on Supported Au, Pd and PdAu Nanoparticle-Based Catalysts

Dmitrii German ¹, Vladislav Turyanskiy ², Julia Schroeder ³, Mohammed Al-Yusufi ³, Katja Neubauer ³, Angela Köckritz ³, Sónia A. C. Carabineiro ^{4,5}, Ekaterina Kolobova ^{1,*} and Alexey Pestryakov ^{1,*}

- ¹ Research School of Chemistry and Applied Biomedical Sciences, National Research Tomsk Polytechnic University, Lenin Av. 30, 634050 Tomsk, Russia; germandmitry93@gmail.com
- ² Research Laboratory "Radioecology and Marine Radiochemistry", Sevastopol State University, st. Universitetskaya 33, 299053 Sevastopol, Russia; morsavinv@bk.ru
- ³ Leibniz Institute for Catalysis, Albert-Einstein Street 29a, 18059 Rostock, Germany; julia.schroeder@catalysis.de (J.S.); mohammed.al-yusufi@catalysis.de (M.A.-Y.); katja.neubauer@catalysis.de (K.N.); angela.koeckritz@catalysis.de (A.K.)
- ⁴ LAQV-REQUIMTE, Department of Chemistry, NOVA School of Science and Technology, Universidade NOVA de Lisboa, 2829-516 Caparica, Portugal; sonia.carabineiro@fct.unl.pt
- ⁵ Centro de Química Estrutural, Institute of Molecular Sciences, Instituto Superior Técnico, Universidade de Lisboa, Av. Rovisco Pais, 1049-001 Lisboa, Portugal
- * Correspondence: ekaterina_kolobova@mail.ru (E.K.); pestryakov2005@yandex.ru (A.P.)

Abstract: The oxidative C-C cleavage of a C₁₈ substrate is an important transformation in synthetic organic chemistry, facilitating the synthesis of valuable C₈-C₉ acids widely used in many industries. Through a comparative analysis of the catalytic and physicochemical properties of catalysts, comprising mono- (Pd or Au) and bimetallic (PdAu) nanoparticles deposited on oxides, oxyhydroxides and graphite-like carbon material Sibunit (Cp), it was shown that the efficiency of the catalyst in the oxidative cleavage of 9,10-dihydroxystearic acid relies on the nature of the active component, the support and the average size of metal nanoparticles (NPs). The dependency of 9,10-DSA conversion on the average size of metal NPs shows the structural sensitivity of the oxidative cleavage reaction. Notably, catalysts with an average size of gold particles less than 3 nm exhibit the highest activity. The nature of the active component and the support material are crucial factors determining the process selectivity. Among the catalysts studied, the most effective for the oxidative cleavage of 9,10-DSA is a material based on Au NPs deposited on Cp.

Keywords: oxidative C-C cleavage; 9,10-dihydroxystearic acid; supported metal NPs; structural sensitivity



Citation: German, D.; Turyanskiy, V.; Schroeder, J.; Al-Yusufi, M.; Neubauer, K.; Köckritz, A.; Carabineiro, S.A.C.; Kolobova, E.; Pestryakov, A. Oxidative Cleavage of 9,10-Dihydroxystearic Acid on Supported Au, Pd and PdAu Nanoparticle-Based Catalysts. *Reactions* **2024**, *5*, 120–134. <https://doi.org/10.3390/reactions5010006>

Academic Editor: Ioannis V. Yentekakis

Received: 4 December 2023
Revised: 16 January 2024
Accepted: 23 January 2024
Published: 27 January 2024



Copyright: © 2024 by the authors. Licensee MDPI, Basel, Switzerland. This article is an open access article distributed under the terms and conditions of the Creative Commons Attribution (CC BY) license (<https://creativecommons.org/licenses/by/4.0/>).

1. Introduction

Nowadays, the importance of developing new sources of energy and chemicals cannot be overestimated. According to British Petroleum (BP) [1], Earth's oil reserves amount to ~1.7 trillion barrels. At the current consumption rate, this supply should only last for 47 years, i.e., until 2070. Additionally, according to a previous BP report [2], natural gas reserves are expected to last until 2069. Thus, the search for new renewable resources is extremely relevant, as confirmed by numerous studies in this direction [3–9].

Biomass emerges as a sustainable alternative, capable of replacing conventional raw materials in an environmentally friendly manner. Statistics show that in 2015, the world produced 11.9 billion tons of biomass, with 61% originating from agriculture and 39% from forestry [10]. Various methods can be employed to extract fatty acids from agricultural raw materials [11–13]. Subsequently, these fatty acids find applications in diverse fields, such as oilfields, organic synthesis, medicine and polymer production [14–17]. Nevertheless, an

alternative and promising approach involves the catalytic cleavage oxidation of biomass-derived fatty acids to produce valuable organic compounds, such as azelaic, pelargonic, suberic and caprylic acids.

Azelaic acid (AA) has applications in several industries. In cosmetics, it is used to treat acne, reduce inflammation and improve skin texture. In pharmaceuticals, AA is a component of medications used in the treatment of various skin diseases. In addition, the potential for using AA as a monomer to create biodegradable plastics is substantial, suggesting its role in the development of environmentally friendly materials [11], suggesting its role in the development of environmentally friendly materials [18].

Pelargonic acid (PA) is applied in agriculture for the production of weed and pest control agents. In addition, PA can be used in the manufacture of paints and coatings with enhanced properties [19,20].

Both suberic acid (SA) and caprylic acid (CA) have a wide range of medical applications. SA can be used as an inhibitor of angiogenesis (formation of new blood vessels), a crucial aspect in the treatment of some diseases. CA has potential applications as an antimicrobial agent or fat burner, which makes it valuable in the therapy of various ailments [21,22].

In industry, the above-mentioned acids are typically obtained through methods characterized by a range of significant disadvantages, including the use of explosion and fire hazardous reagents, the generation of toxic waste and the implementation of complex technological schemes [23,24]. For example, the production of AA and PA involves the ozonolysis of oleic acid or linoleic acid, introducing potential hazards due to the use of flammable and toxic ozone [23]. In the case of SA and CA, the production process uses nitric acid as an oxidizing agent, which contributes to the formation of poisonous NO and NO₂ [24]. An alternative approach to produce these acids is the oxidation of biomass-derived substrates using various catalytic systems (Table 1).

Table 1. Production of azelaic and pelargonic acids from various substrates.

№	Substrate *	Catalyst	Conditions	Conversion (%)	Yield or Selectivity (%)				Ref.
					AA	PA	SA	CA	
1	MDS	Au/Al ₂ O ₃	1 mmol of substrate, 0.2 mol % Au, 5 mmol NaOH, 20 mL H ₂ O, 80 °C, 5 bar O ₂	100	86	99	~7	~7	[25]
2	9,10-DHSA	CoAc ₂ / H ₂ WO ₄ / CH ₃ COONa	360 min, 15 bar O ₂ , 70 °C	100	15	56	-	-	[26]
3	HOSO	CeO ₂ / Nb ₂ O ₅ / TiO ₂ + MeOH	12 bar O ₂ (180 °C), 6 bar N ₂ (160 °C), 5 h	-	34				[27]
4	OA	Silica-supported W-oxide	20 g of substrate, 60 mL H ₂ O ₂ (30%), 150 mL tert-butanol, 1.5 g of catalyst, 130 °C, 1 h	79	32	36	-	-	[28]
5	OA	H ₂ WO ₄	5 g of substrate, 7.5 g H ₂ O ₂ (60%), ratio cat/sub = 1/400, 100 °C, 24 h	94	60	16	-	-	[29]
6	OA	[Fe(OTf) ₂ (6-Me-PyTACN)]	Solvent – MeCN, 4.5 eq. NaIO ₄ , 100 eq. H ₂ O, 24 h, then H ₂ SO ₄ (0.5 eq.) in H ₂ O (50 eq.), 12 h, and NaHCO ₃ (1 eq.) and catalyst (1 mol %)	100	85	-	-	-	[30]
7	OA	Cr/MCM-41	1 g of substrate, 40 mg of catalyst, 180 °C, 8 h, pO ₂ = 1 Mpa and pCO ₂ = 10 MPa	>95	32	32	10	10	[31]

Table 1. Cont.

№	Substrate *	Catalyst	Conditions	Conversion (%)	Yield or Selectivity (%)				Ref.
					AA	PA	SA	CA	
8	9,10-DSTG	CuFe ₂ O ₄	1 wt% catalyst, 80 °C, stirring 500 rpm, pO ₂ = 25 bar, 5 h	96	70	52	-	-	[18]
9	OA	-	2 g of substrate, flow rate for OA 1 mL/min, flow rate for O ₃ /O ₂ 500 mL/min, 0 °C, solvent—50 mL of acetone:H ₂ O (95:5)	-	84	-	-	-	[32]
10	SO	V ₂ O ₅ /TiO ₂	1 g of substrate, 30 wt. % of catalyst, TBHP (20 volume), 80 °C, 12 h	-	66	-	-	-	[33]
11	VDFE	Ru(OH) _x /γ-Al ₂ O ₃	4 g of substrate, 12 mL dodecane, 60 mL H ₂ O, 6 mol % of catalyst, pO ₂ = 5 bar	99	83	86	6	4	[34]
12	OA	KMnO ₄ /NaOH/TEBAC	2 g of substrate, 2 g of KMnO ₄ , 0.2 g TEBAC, 50 mL H ₂ O, 50 °C, 8 h	100	96	81	-	-	[35]
13	OA	WO ₃ ·H ₂ O	1 g of substrate, 7.5 mL of tert-butanol, 4 mL of H ₂ O ₂ , 0.45 g of catalyst, stirring 400 rpm, 120 °C, 5 h	100	77	69	-	-	[36]
14	OA	Surfactant-capped NPs WO ₃	2 g of substrate, 15 mL of tert-butanol, 6 mL of H ₂ O ₂ , 0.9 g of catalyst, 120 °C, 5 h	95	58	24	-	-	[37]
15	OA	ACO-Ru (2%)	0.5 mmol of substrate, solvent—H ₂ O/MeCN/AcOEt (4/2/1), 8 equivalents of NaIO ₄ , 100 mg of catalyst, stirring 1500 rpm, r.t., 24 h	53	16	16	-	-	[38]
16	OA	CBO-Ru (2%)	0.5 mmol of substrate, solvent—H ₂ O/MeCN/AcOEt (4/2/1), 8 equivalents of NaIO ₄ , 100 mg of catalyst, stirring 1500 rpm, r.t., 24 h	100	75	75	-	-	[38]

* MDS—methyl-9,10-dihydroxystearate; 9,10-DHSA—9,10-dihydroxystearic alcohol; HOSO—High oleic sunflowers oil; OA—Oleic acid; 9,10-DSTG—9,10-Dihydroxystearic triglyceride; SO—Triadica sebifera seed oil; VDFE—Vicinal diol fatty esters.

In the considered studies, various catalytic systems and substrates were used for the synthesis of C₈-C₉ acids. The best result was obtained using the Au/Al₂O₃ catalyst [25], with a yield of 86% for AA and 99% for PA, with minimal formation of SA and CA. The high activity of the catalyst in this study is attributed to the small size of gold nanoparticles and their interaction with the support surface. However, other physicochemical properties of the catalyst and their influence on the oxidative C-C cleavage activity of the C₁₈ substrate were not explored. Additionally, when using Al₂O₃ as a support, its instability in an alkaline medium should be taken into account [39].

Table 1 also presents the results of other studies [30,34,35,38], where relatively high yields of AA (75–96%) and PA (69–86%) were obtained. Nevertheless, these described catalysts either involve complex multicomponent systems or operate under specific process conditions, which imposes certain difficulties in their practical implementation.

Thus, it is obvious that in order to establish scientifically grounded approaches to select the most effective, economical, environmentally feasible and technically viable methods to intensify biomass processing into valuable chemical products, it is necessary to conduct systematic studies. This is particularly relevant to the choice of catalyst, also taking into account issues related to its deactivation [40–47] and, accordingly, the choice of its operating

conditions. Therefore, the aim of this work is to elucidate the catalyst characteristics that determine its efficiency in the oxidative cleavage process of 9,10-dihydroxystearic acid. This investigation focuses on mono- (Pd or Au) and bimetallic (Pd-Au) nanoparticles deposited on oxides, oxyhydroxides and graphite-like carbon material Sibunit (Cp) through a comparative analysis of their catalytic and physicochemical properties.

2. Materials and Methods

As catalytic systems for the comparative study, Au/AlOOH_S5, Au/AlOOH_C, Au/La₂O₃/TiO₂, Au/CeO₂/TiO₂, Pd/Cp-NH₄OH, Au/Cp-NH₄OH and PdAu/Cp-NH₄OH materials were chosen. These materials previously demonstrated efficiency as catalysts in processes such as low-temperature CO oxidation and liquid-phase oxidation of n-octanol, glycerol, 5-HMF and betulin [39,48–52]. Other than Au/Cp-NH₄OH material, it is used for the first time. They exhibit significant variations in their physicochemical properties.

2.1. Preparation of Supports and Synthesis of Catalysts

2.1.1. Modification of Titanium Oxide

Titania Degussa P25 (45 m²/g, nonporous, 70% anatase and 30% rutile, purity > 99.5%, Merck, Darmstadt, Germany) was used as starting support. MeTiO₂ supports with a molar ratio Ti/Me = 40 (where Me represents La or Ce) were synthesized by impregnation of the initial titanium oxide with aqueous solutions of La(NO₃)₃·6H₂O and Ce(NO₃)₃·6H₂O nitrates (Merck, Darmstadt, Germany). Subsequently, the samples were dried at room temperature for 48 h and at 110 °C for 4 h, followed by calcination at 550 °C for 4 h.

2.1.2. Modification of Sibunit

Sibunit (CNCT BIC, Omsk, Russia) was modified with NH₄OH as follows: boiling in 20 wt. % nitric acid solution for 1 h, then washed with distilled water and dried at 80 °C for 2 h.

2.1.3. Synthesis of Catalysts

Gold (4% by weight) was deposited on metal oxides using a deposition precipitation method with urea at 80 °C for 16 h, in the absence of light [53–56], using H₂AuCl₄·3H₂O (Merck, Darmstadt, Germany) as the gold precursor. In order to decompose the hydrolysis products of the gold (III) complex with urea on the support surface, the synthesized catalysts were pretreated in a hydrogen atmosphere at 300 °C for 1 h (15% of H₂ in Ar, flow rate 300 mL/min).

Monometallic catalysts containing 1 wt. % Au or Pd were synthesized using the sol immobilization method [57]. In this process, 1 mL of Na₂PdCl₄ (Merck, Darmstadt, Germany) or H₂AuCl₄·3H₂O (Merck, Darmstadt, Germany) solution containing 10 mg of Pd or Au in the count of pure metal and 0.5 mL of a solution containing 1 wt. % PVA (Merck, Darmstadt, Germany) was introduced into a certain volume of water. After 5 min, 0.1 M NaBH₄ solution (Merck, Darmstadt, Germany) was rapidly injected under vigorous stirring, with the metal:NaBH₄ ratio at 1:4 mol/mol. After 30 min, a sample of support required for obtaining a catalyst with 1 wt. % metal content and a few drops of H₂SO₄ (Panreac AppliChem, Barcelona, Spain) was added to the obtained sol. Deposition of nanoparticles was carried out for 1 h, and then the catalyst powder was thoroughly washed with deionized water and dried at 80 °C for 2 h in air atmosphere.

The bimetallic PdAu catalysts were prepared similarly to the monometallic synthesis method previously described. To a defined amount of water, 684 μL of Na₂PdCl₄ solution (10 mg Pd/1 mL H₂O), 316 μL of H₂AuCl₄·3H₂O solution (10 mg Au/1 mL H₂O) and 0.5 mL of a solution containing 1 wt. % PVA were added. After 5 min, under vigorous stirring, 0.1 M NaBH₄ solution was rapidly injected into the solution, with the metal:NaBH₄ ratio at 1:4 mol/mol. After 30 min, a weight of support required to prepare a catalyst containing 1 wt. % metal and a few drops of H₂SO₄ was added to the obtained sol. Deposition of

nanoparticles was carried out for 1 h, then the catalyst powder was thoroughly washed with deionized water and dried at 80 °C for 2 h in an air atmosphere.

2.2. Synthesis of 9,10-Dihydroxystearic Acid

For the dihydroxylation of oleic acid, an oxidizing mixture was prepared as follows: 250 mL of tert-butanol (Merck, Darmstadt, Germany) and 105 mL of 30% H₂O₂ solution (Merck, Darmstadt, Germany) were added to a three-neck flask equipped with a reflux condenser, overhead stirrer and thermometer. In addition, 69.9 g of anhydrous MgSO₄ (Merck, Darmstadt, Germany) was gradually added in portions. The reaction mixture was stirred for 4 h at 30 °C. The temperature of reaction was controlled using an ice bath. The obtained solution was then filtered on a vacuum station.

Subsequently, 0.71 g of methyltrioxorhenium (Merck, Darmstadt, Germany) and 99 g of oleic acid were dissolved in 210 mL of the resulting oxidizing solution. The dihydroxylation process was performed for 48 h at 40 °C.

At the end of the process, to neutralize the residual H₂O₂, a suspension of NaHSO₃ (Merck, Darmstadt, Germany) was added to the reaction mixture, and a special indicator paper was used to check for remaining H₂O₂. After neutralization, tert-butanol was removed using a rotary evaporator, and the precipitate was dissolved in 500 mL of heptane (Merck, Darmstadt, Germany). The resulting solution was left in the refrigerator for 24 h at −5 °C. Then, the precipitate was filtered off, washed with petroleum ether (40–60 °C fraction) and dried under vacuum.

2.3. Catalytic Experiments

The autoclave reactor was charged with 0.317 g of 9,10-dihydroxystearic acid, a catalyst loading (metal/substrate ratio is 1:500 mol/mol) and 20 mL of 0.25 M NaOH solution (Merck, Darmstadt, Germany). Subsequently, the reactor was purged with argon several times and heated to the desired temperature at 2 atm of Ar while stirring at 200 rpm. Once the temperature reached 80 °C, 5 atm of O₂ were pressurized into the reactor, stirring was adjusted to 1500 rpm and the reaction was carried out for 260 min. Scheme of reaction is shown in Figure 1.

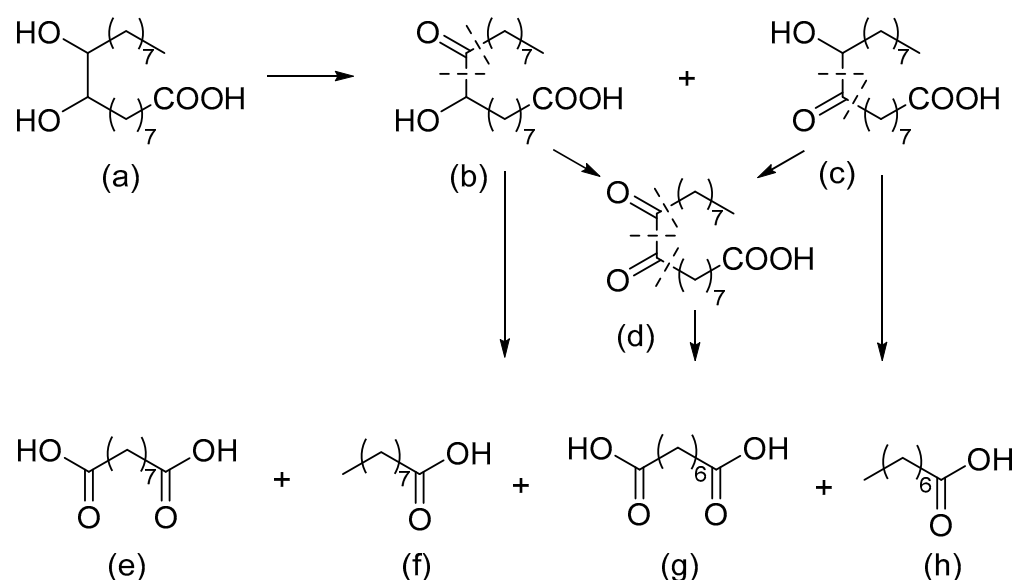


Figure 1. Oxidative cleavage of 9,10-dihydroxystearic acid: (a)—9,10-dihydroxystearic acid; (b)—9-hydroxy-10-oxostearic acid; (c)—10-hydroxy-9-oxostearic acid; (d)—9,10-dioxostearic acid; (e)—azelaic acid; (f)—pelargonic acid; (g)—suberic acid; (h)—caprylic acid. Reproduced from [58] with permission from the Royal Society of Chemistry.

After the designated time elapsed, the reaction mixture was cooled to room temperature and then filtered from the catalyst using a vacuum station. The filter was washed with 25 mL of 0.1 M NaOH solution and 50 mL of distilled water to extract any remaining reaction products. To precipitate the obtained acids, an aqueous HCl solution was added to the filtered mixture until reaching pH values of 2–3. To transfer the reaction products and unreacted substrate to the organic solvent, the resulting solution was placed in a separating funnel, and 15 mL of methyl tert-butyl ether (Acros Organics, Verona, Italy) was added. The solution was shaken, left to stand for a few minutes and drained. This procedure was repeated 5 times. In the solution, 10 g of anhydrous MgSO₄ (Merck, Darmstadt, Germany) was added to remove the residual water and left for 2 h at room temperature. When the time elapsed, the mixture was filtered and transferred to a measuring flask, and the volume of the solution was adjusted to 100 mL with methyl tert-butyl ether.

From the final mixture, 1 mL was taken, and the methyl tert-butyl ether was removed using a rotary evaporator. Then, 250 µL of silylating agent was added, and the silylation process was carried out for 1 h at 80 °C. The solution with silylated products was transferred to a 2 mL volumetric flask. The required amount of the standard—diethylene glycol dibutyl ether (Merck, Darmstadt, Germany)—was added and brought to the mark with methyl tert-butyl ether. The reaction products were analyzed by a GC-MC Shimadzu GCMS-QP2010S (Shimadzu Corp., Kyoto, Japan) chromatograph on a Rtx-5MS column (30 m × 0.25 mm × 0.25 µm) manufactured by BGB Analytik (Boeckten, Switzerland).

To check the material balance, the recovery rate was calculated, indicating how much of the substrate (i.e., 9,10-dihydroxystearic acid) was converted into the target products or remained unreacted. The recovery rate is estimated as the sum of moles of all products and unreacted substrate divided by the original number of substrate moles and multiplied by 100%:

$$\text{Recovery rate} = \frac{\sum \eta \text{ products} \cdot 0.5 + \eta \text{ substrate}}{\eta_0 \text{ substrate}} \times 100\%, \quad (1)$$

where “ $\sum \eta \text{ products}$ ” is the total number of moles of products formed, “ $\eta \text{ substrate}$ ” is the number of moles of unreacted substrate, “ $\eta_0 \text{ substrate}$ ” is the number of moles of substrate before the reaction.

To evaluate the activity of the synthesized catalysts, the conversion and product yields were calculated using the following equations:

$$\text{Conversion} = \frac{\eta_0 \text{ substrate} - \eta \text{ substrate}}{\eta_0 \text{ substrate}} \times 100\%, \quad (2)$$

where “ $\eta \text{ substrate}$ ” is the number of moles of unreacted substrate, and “ $\eta_0 \text{ substrate}$ ” is the number of moles of substrate before the reaction.

$$\text{Yield} = \frac{\eta \text{ product}}{\eta_0 \text{ substrate}} \times 100\%, \quad (3)$$

where “ $\eta \text{ product}$ ” is the number of moles of product formed, and “ $\eta_0 \text{ substrate}$ ” is the number of moles of substrate before the reaction.

Turnover frequency was calculated with regard to the number of moles of metal as follows:

$$\text{TOF} = \frac{\text{conversion} \times \eta_0 \text{ substrate}}{\eta \text{ metal} \times 100 \times 4.33 \text{ h}}, \quad (4)$$

where “ $\eta_0 \text{ substrate}$ ” is the number of moles of substrate before the reaction, and $\eta \text{ metal}$ represents metal content in the catalyst weight.

2.4. Characterization of Catalysts and Supports

The mass fractions of gold and palladium were determined by atomic emission spectroscopy with inductively coupled plasma (AES ICP) using a Thermo Scientific iCAP 6300 Duo spectrometer (Thermo Fisher Scientific, Waltham, MA, USA) and X-ray energy dispersive spectroscopy (XEDS) in a JEOL JEM-2100F (JEOL Ltd., Tokyo, Japan)

electronic microscope. The specific surface area, pore size and pore volume of the catalysts and corresponding supports were investigated using the low-temperature nitrogen adsorption–desorption method on a Micromeritics 23x-Tristar 3000 Apparatus (Micromeritics Instrument Corporation, Norcross, GA, USA). The phase composition of the supports and catalysts was analyzed by X-ray phase analysis on Philips XPert PRO (Philips, Amsterdam, The Netherlands) and Bruker D8 (Bruker Corp., Billerica, MA, USA). The electronic state of gold and palladium on the surface of catalysts was studied by X-ray photoelectron spectroscopy on ESCALAB 200A (Thermo Fisher Scientific, Waltham, MA, USA) and SPECS GmbH custom-made system using a PHOIBOS 150 WAL (SPECS Surface Nano Analysis GmbH, Berlin, Germany). The size and distribution of gold and palladium nanoparticles were analyzed by transmission electron microscopy on a JEOL JEM-2100F instrument (JEOL Ltd., Tokyo, Japan). More details of the methods used for the study of supports and catalysts are described in the Supplementary Material.

3. Results

The physicochemical properties of the samples used in this work are detailed in our previous publications [39,48–52] and summarized in Table 2, with graphical representations presented in Figures S1–S4 in Supplementary Information. With the exception of the data for Au/Cp-NH₄OH material, they are presented for the first time.

Table 2. Physicochemical characteristics of supports and corresponding catalysts [39,48–52].

Sample	Indicated Phase ^a	w _i /Σw (%) ^a	S _{BET} (m ² /g) ^b	Pore Size (nm) ^b	Pore Volume (cm ³ /g) ^b	Metal Content (wt. %) ^c		d _{NPs} (nm) ^d	Relative Content (%) ^e					
						Pd	Au		Pd			Au		
									Pd ⁰	Pd ²⁺	Pd ⁴⁺	Au ⁰	Au ⁺	Au ³⁺
AlOOH_S5	AlO(OH) (orthorhombic)	100	385	5.7	0.67	-	-	-	-	-	-	-	-	-
AlOOH_C	AlO(OH) (orthorhombic)	100	321	5.8	0.41	-	-	-	-	-	-	-	-	-
Au/AlOOH_S5	AlO(OH) (orthorhombic)	96	293	6.0	0.55	-	3.94	4.2	-	-	-	100	0	0
	Au	4												
Au/AlOOH_C	AlO(OH) (orthorhombic)	96	254	5.6	0.52	-	3.95	2.9	-	-	-	81	19	0
	Au	4												
La ₂ O ₃ /TiO ₂	TiO ₂ (tetragonal)	-	45.3	356.3	0.38	-	-	-	-	-	-	-	-	-
CeO ₂ /TiO ₂	TiO ₂ (tetragonal)	-	43.4	292.4	0.35	-	-	-	-	-	-	-	-	-
	CeO ₂ (cubic)	-												
Au/La ₂ O ₃ /TiO ₂	TiO ₂ (tetragonal)	-	45.2	211.5	0.24	-	3.3	2.6	-	-	-	83	17	0
Au/CeO ₂ /TiO ₂	TiO ₂ (tetragonal)	-	46.6	211.1	0.26	-	4.1	2.8	-	-	-	68	20	12
Cp-NH ₄ OH	C (hexagonal)	-	318	6.4	0.58	-	-	-	-	-	-	-	-	-
Pd/Cp-NH ₄ OH	C (hexagonal)	-	320	6.8	0.62	1.2	-	4.3	59	31	10	-	-	-
	Pd (cubic)	-												
Au/Cp-NH ₄ OH	C (hexagonal)	-	322	5.0	0.55	-	0.9	2.9	-	-	-	100	0	0
PdAu/Cp-NH ₄ OH	C (hexagonal)	-	331	6.5	0.62	0.56	0.20*	4.0	91	7	2	92	8	0

w_i/Σw—mass fraction of the phase according to XRD; S_{BET}—specific surface area calculated by BET method; d_{NPs}—average diameter of nanoparticles; ^a XRD; ^b N₂ adsorption–desorption; ^c AES ICP; ^d HRTEM; ^e XPS; *—determined by XEDS.

3.1. X-ray Diffraction

The structural characteristics of the supports and the corresponding catalysts were determined by XRD (Figure S3, Table 2).

The $2\theta = 14.1^\circ, 28.2^\circ, 38.4^\circ, 49.3^\circ, 65.0^\circ$ and 72.2° reflections observed in the X-ray diffraction patterns of aluminum supports (AlOOH_S5 and AlOOH_C) belong to aluminum oxyhydroxide (boehmite) with an orthorhombic crystal lattice [59]. It should be noted that according to the manufacturer's data, AlOOH_S5 material is a mixture of 5% SiO₂ and 95% boehmite, but no reflexes related to SiO₂ were detected, possibly due to the amorphous structure of the silicon oxide included in the material. Gold deposition did not lead to any structural changes in these supports. A gold phase was identified for both catalysts at $2\theta = 44.3^\circ$ and 77.7° [60]. The gold content determined using the Rietveld method agreed well with the AES ICP data (Table 2).

The X-ray diffraction patterns of La₂O₃/TiO₂ and CeO₂/TiO₂ supports show reflections corresponding to the phases of rutile ($2\theta = 27.6^\circ$ and 41.5°) and anatase ($2\theta = 25.5^\circ, 38.0^\circ, 48.2^\circ, 62.9^\circ$ and 75.2°) [61]. Additionally, diffraction peaks at $2\theta \sim 28.6^\circ$ and 33.1° belonging to the CeO₂ phase were observed [62]. The analysis of the phase composition of the related catalysts revealed no changes in the structure of the supports after gold deposition. In addition, no reflexes belonging to the gold phase were detected, possibly attributable to the small size of gold NPs (below the sensitivity level of the method) and their uniform distribution on the support surface or to their X-ray amorphous structure.

The XRD spectra of carbon samples showed diffraction maxima at $2\theta = 25.5^\circ$ and 43.2° , which is consistent with literature data corresponding to the carbon material "Sibunit" [63]. The deposition of gold and/or palladium did not change the structure of the support. Notably, no reflexes belonging to the deposited metals were found on the diffractograms measured for Au/Cp-NH₄OH and PdAu/Cp-NH₄OH catalysts. The exception is Pd/Cp-NH₄OH, where maxima were observed at $2\theta = 40.0^\circ$ and 68.5° , corresponding to the palladium phase [64].

3.2. AES ICP and XEDS

According to AES ICP data, gold was deposited on the surface of boehmite, and titanium oxide was modified with cerium oxide in an amount close to nominal (Table 2). However, in the case of TiO₂-modified La₂O₃ and Sibunit, the completeness of gold deposition is below nominal, specifically 67% for Au/La₂O₃/TiO₂, 90% for Au/Cp-NH₄OH and 83% for PdAu/Cp-NH₄OH. It is worth noting that the completeness of metal deposition is influenced by many factors, such as the nature of the metal precursor, method of preparation and nature of the support (hydride, hydroxyl, carbonyl, carboxyl and other groups, i.e., functional surface coverage, point of zero surface charge). In addition, the functional coating of the support may change due to reagents used in catalyst synthesis, affecting the amount of metal deposition. A specific cause cannot be established based on the available experimental data.

For Pd/Cp-NH₄OH and PdAu/Cp-NH₄OH, the completeness of palladium deposition was 100 and 80%, respectively. In the case of the bimetallic catalyst, competitive adsorption of metal precursors during synthesis might occur.

3.3. N₂ Adsorption–Desorption

According to the data presented in Table 2, the initial boehmite and Sibunit, along with their corresponding catalysts, are mesoporous materials with extended specific surface area. However, for AlOOH_S5 and AlOOH_C materials, gold deposition on their surface results in a significant decrease in the specific surface area of the synthesized catalysts. This reduction may be a consequence of an increase in the average size of support crystals due to agglomeration during catalyst synthesis and a decrease in the available pores.

CeO₂- and La₂O₃-modified TiO₂ and their corresponding catalysts exhibit a macroporous structure with considerably lower specific surface area values compared to boehmite and Sibunit materials.

3.4. Transmission Electron Microscopy

The size distribution of the metal particles and TEM images are shown in Figure S4, and the values of the average sizes of metal NPs are summarized in Table 2.

For gold catalysts deposited on AlOOH_S5 and AlOOH_C, the average nanoparticle sizes were 4.2 nm and 2.9 nm, respectively. The significantly larger size of gold nanoparticles on the boehmite Siral 5 is probably due to the presence of SiO₂ in its composition. The existence of SiO₂ potentially alters the point of zero charge on the surface compared to AlOOH_C, leading to a modification in the interaction nature of the gold precursor with the surface of the support [39,65].

For Au/La₂O₃/TiO₂ and Au/CeO₂/TiO₂, the average size of Au nanoparticles (2.6 nm and 2.8 nm) and their distribution range (1–7 nm) are similar.

An analysis of TEM images of carbon samples reveals that the average size of nanoparticles on the surface of Au/Cp-NH₄OH, Pd/Cp-NH₄OH and PdAu/Cp-NH₄OH are 2.9 nm, 4.3 nm and 4.0 nm, respectively. As demonstrated in [66], the reduction rate of the metal precursor plays a crucial role in the nucleation and growth processes, serving as one of the main factors influencing the final size and shape of the NPs. The rate of metal atom generation is influenced by the nature of the precursor and reducing agent. In this case, HAuCl₄·3H₂O and Na₂PdCl₄ were used as gold and palladium precursors, with NaBH₄ acting as the reducing agent. The oxidizing potential of NaBH₄ strongly depends on the solution pH, rising with increasing pH. The elevated oxidizing potential of NaBH₄ is associated with an increase in its reduction capacity. Consequently, the differing reduction rates of gold and palladium precursors likely contribute to the observed variations in the average size of gold and palladium NPs, as well as their mixture.

3.5. X-ray Photoelectron Spectroscopy

The results detailing the electronic state of gold and palladium on the surface of the investigated catalysts are presented in Table 2 and Figures S1 and S2.

On the surfaces of Au/AlOOH_S5 and Au/Cp-NH₄OH materials, gold is only present in the metallic state. However, for all other samples, along with the metallic state, an additional gold state, Au⁺, was detected. The contribution of Au⁺ increases in the following sequence: PdAu/Cp-NH₄OH (8%), Au/La₂O₃/TiO₂ (17%), Au/AlOOH_C (19%) and Au/CeO₂/TiO₂ (20%). Moreover, in addition to Au⁰ and Au⁺, Au³⁺ (12%) was also found on the surface of Au/CeO₂/TiO₂ material.

The deconvolution of Pd 3d XRD spectra revealed that palladium on the surface of Pd/Cp-NH₄OH and PdAu/Cp-NH₄OH catalysts is present in three states: Pd⁰, Pd²⁺ and Pd⁴⁺. A significant portion is in the metallic state, namely 59% for monometallic and 91% for bimetallic catalysts. In the case of Pd/Cp-NH₄OH, the involvement of Pd²⁺ and Pd⁴⁺ states accounts for 31% and 10%, respectively, while for PdAu/Cp-NH₄OH, the corresponding amounts are 7% and 2%.

3.6. Catalysis

The activity of the investigated catalysts in the process of oxidative C-C cleavage was evaluated under the following conditions: 0.317 g (1 mmol) of the substrate, Me/substrate ratio = 1:500, 20 mL of 0.25 M NaOH solution, T = 80 °C, p = 5 bar O₂, t = 260 min, stirring 1500 rpm. The catalytic data are presented in Table 3.

For gold deposited on aluminum oxyhydroxides (Table 3, entries 1 and 2), the catalyst with boehmite Catapal B as the support for gold NPs exhibited the highest activity. This catalyst achieved 100% conversion of 9,10-DSA with a recovery rate of 69%. In contrast, the Au/AlOOH_S5 material showed nearly three times lower conversion (35%) but a higher recovery rate (83%). Similarly, the yield of products was also higher for Au/AlOOH_C, with 51% for azelaic acid and 66% for pelargonic acid, along with small amounts of caprylic and suberic acids (11% and 9%, respectively). These observed variations in catalytic behavior can be attributed to the structural sensitivity of the oxidative C-C cleavage reaction, considering the significantly smaller size of Au NPs on the Au/AlOOH_C surface compared to

Au/AlOOH_S5 (2.9 nm and 4.2 nm, respectively) (Table 2, Figure S4). The influence of the average size of gold NPs on the catalytic properties of Au NP catalysts in oxidative C-C cleavage was also observed in previous studies [25].

Table 3. Results of catalytic experiments.

Entry	Catalyst	Conv., (%)	Y AA, (%)	Y PA, (%)	Y CA, (%)	Y SA, (%)	Recovery Rate
1	Au/AlOOH_S5	35	11	19	4	3	83
2	Au/AlOOH_C	100	51	66	11	9	69
3	Au/La ₂ O ₃ /TiO ₂	99	51	56	7	7	62
4	Au/CeO ₂ /TiO ₂	100	29	37	6	7	40
5	Pd/Cp-NH ₄ OH	46	0	0	0	0	54
6	Au/Cp-NH ₄ OH	88	48	61	21	14	84
7	PdAu/Cp-NH ₄ OH	77	0	0	0	0	23

Reaction conditions: 0.317 g (1 mmol) of substrate, ratio Me/substrate = 1:500, 20 mL of 0.25 M NaOH solution, T = 80 °C, p = 5 bar O₂, t = 260 min, stirring 1500 rpm. Conv.—conversion; Y AA—yield of azelaic acid; Y PA—yield of pelargonic acid; Y CA—yield of caprylic acid; Y SA—yield of suberic acid.

Additionally, it is essential to consider the different chemical compositions of the supports and, consequently, their different functional coatings, which play a crucial role in this kind of reaction. This might explain the observed values of the recovery rate. With a substrate conversion of 100% and a recovery rate of 69%, it is evident that a portion of 9,10-DSA converts not only to the target products. Thus, side reactions catalyzed by the acid-base sites of the support also likely take place on the catalyst surface. An example of a side reaction catalyzed by functional groups of the support, particularly its strong acid-base sites, is the oxidation of betulin on Au/alumina supports. The products of this reaction were oligomers/polymers that remained on the catalyst surface and, thus, were not detected by chromatography [39].

Similar to the case of Au/AlOOH_C material with an average gold particle size of 2.9 nm, Au/La₂O₃/TiO₂ and Au/CeO₂/TiO₂ catalysts with an average gold particle size of 2.6 and 2.8 nm, respectively, showed high activity in the oxidative C-C cleavage process, achieving 99% and 100% conversion of 9,10-DSA, respectively (Table 3, entries 3 and 4). However, the yields of AA and PA (with a similar ratio between them for each of the catalysts), as well as the recovery rate, were different among these catalysts. Specifically, for the Ce-modified sample, these values are, on average, 20 points lower than for the La-modified sample. One possible explanation for the observed differences in Au/La₂O₃/TiO₂ and Au/CeO₂/TiO₂ could be attributed to the electronic state of gold on the surface of these supports. For La₂O₃-modified TiO₂, more than 80% of gold exists in the metallic state, whereas for CeO₂-modified TiO₂, it is 68% (Table 2). Additionally, on the surface of CeO₂-modified TiO₂, in addition to Au⁺, which exhibits similar content for both supports, there is also Au³⁺. Another potential factor contributing to the variations is the different functional coatings of La₂O₃- and CeO₂-modified TiO₂ supports, which determines the acid-base properties of the materials. This, in turn, may be responsible for selectivity; in this case, the recovery rate, as noted above, serves as an indicator.

Among carbon catalysts (Table 3, entries 5–7), the generation of target products from the oxidative cleavage reaction of 9,10-DSA was exclusively observed for Au/Cp-NH₄OH. It is noteworthy that despite incomplete substrate conversion (88% conversion), this sample exhibits the highest recovery rate (84%) among all the catalysts studied. As it is known, graphite (Sibunit—mesoporous graphite-like carbon material) is a chemically inert substance. Its functionalization with strong acids or bases, leading to the formation of defects, serves mainly to stabilize the NPs immobilized on its surface. At the same time, during functionalization on the surface of carbon, carboxyl, carbonyl and other groups are formed, but these groups are usually much weaker than the acid-base sites found on the surface of oxide materials. Thus, it can be assumed that the high recovery rate values observed for Au/Cp-NH₄OH are likely due to the unique features of the ammonia-modified Sibunit

functional coating, and gold NPs with an average size ≥ 3 nm are responsible for the activity, as in the cases of Au/AlOOH_C, Au/La₂O₃/TiO₂ and Au/CeO₂/TiO₂ materials.

It should be noted that Pd/Cp-NH₄OH and PdAu/Cp-NH₄OH materials are active in the oxidative C-C cleavage process, with the conversion of 9,10-DSA reaching 46% and 77%, respectively. However, no formation of target products was observed for them (Table 3, entries 5 and 7). A possible explanation could be attributed to the unique properties of palladium, which is capable of absorbing hydrogen generated during intermediate steps or from substrate/intermediates. During the operation of Pd-containing catalysts, released hydrogen might return to the reaction atmosphere, potentially initiating non-target processes. In addition, Pd is a “classical” catalyst for C-C bond formation processes, contributing to the production of off-target products [67–69].

For a more demonstrative confirmation of the hypothesis regarding the structural sensitivity of the oxidative cleavage reaction of 9,10-dihydroxystearic acid, Table 4 includes TOF values compared with the average size of metal NPs. The presented data clearly show that the TOF values for catalysts with particles with an average size of around 3 nm are several times higher than the corresponding values for catalysts characterized by an average particle size of 4 nm or more.

Table 4. TOF dependence on average nanoparticle size.

Entry	Catalyst	Particle Size, nm	TOF, h ⁻¹
1	Au/AlOOH_S5	4.2	40
2	Au/AlOOH_C	2.9	115
3	Au/La ₂ O ₃ /TiO ₂	2.6	114
4	Au/CeO ₂ /TiO ₂	2.8	115
5	Pd/Cp-NH ₄ OH	4.3	53
6	Au/Cp-NH ₄ OH	2.9	101
7	PdAu/Cp-NH ₄ OH	4.0	89

4. Conclusions

This study focused on comparatively evaluating the catalytic properties of materials with significantly different physicochemical characteristics in the oxidative C-C cleavage of the C₁₈ substrate.

Regardless of the nature of the support, the most active catalysts were those with an average size of gold NPs below 3 nm (Table 3, Entry 2–4, 6), demonstrating the structural sensitivity of the oxidative cleavage reaction of 9,10-DSA. Simultaneously, the functional coating of the support, depending on its nature, considerably influenced the selectivity of the oxidative C-C cleavage process (yield of target products), including the recovery rate, reflecting the occurrence of nontarget processes. Metal oxyhydroxides (AlOOH_S5 and AlOOH_C) and oxides (La₂O₃/TiO₂ and CeO₂/TiO₂) were found to be inefficient supports for Au-containing catalysts in the oxidative cleavage of 9,10-DSA due to low recovery rate values, consequently promoting nonselective processes. On the other hand, graphite-like carbon material Sibunit, owing to its unique functional cover, allowed us to obtain an Au NPs catalyst exhibiting the highest recovery rate (84%) among all investigated catalysts, achieving a conversion level of 88% for 9,10-DSA. The proximity of substrate conversion and recovery rate values indicates a minimal possibility of non-target processes on Au/Cp-NH₄OH.

Notably, palladium, including in bimetallic system, proved to be an inefficient active component for catalysts in the oxidative cleavage of 9,10-DSA. Similar to Au/AlOOH_S5, Au/AlOOH_C, Au/La₂O₃/TiO₂ and Au/CeO₂/TiO₂ materials, the use of Pd-based catalysts (Pd/Cp-NH₄OH and PdAu/Cp-NH₄OH) led to non-target processes, with this inefficiency being most pronounced in this case.

In summary, the main factors determining the efficiency of the catalyst in the oxidative cleavage of 9,10-DSA include the nature of the active component, the support and the average size of metal NPs.

Supplementary Materials: The following supporting information can be downloaded at: <https://www.mdpi.com/article/10.3390/reactions5010006/s1>, Detailed description of the methods used to characterize the supports and corresponding catalysts. Figure S1. Deconvoluted XPS spectra of Au4f for: Au/AlOOH_C; Au/AlOOH_S5; Au/La₂O₃/TiO₂; Au/CeO₂/TiO₂; Au/Cp-NH₄OH; PdAu/Cp-NH₄OH. Figure S2. Deconvoluted XPS spectra of Pd3d for: Pd/Cp-NH₄OH and PdAu/Cp-NH₄OH. Figure S3. XRD patterns for supports and corresponding catalysts. Figure S4. TEM images and corresponding histograms for: Au/AlOOH_C; Au/AlOOH_S5; Au/La₂O₃/TiO₂; Au/CeO₂/TiO₂; Pd/Cp-NH₄OH; Au/Cp-NH₄OH; PdAu/Cp-NH₄OH.

Author Contributions: Conceptualization, E.K., A.P. and A.K.; methodology, D.G., J.S., K.N., M.A.-Y. and A.K.; investigation, D.G. and V.T.; resources, S.A.C.C. and A.K.; data curation, D.G., V.T., A.K., and E.K.; writing—original draft preparation, D.G. and E.K.; writing—review and editing, D.G., E.K., S.A.C.C. and A.P.; supervision, A.K.; project administration, E.K. and A.P.; funding acquisition, S.A.C.C. and A.P. All authors have read and agreed to the published version of the manuscript.

Funding: The research is funded by the Ministry of Education and Science of the Russian Federation Program No. 075–03–2021–287/6 (Russia). S.A.C.C. acknowledges Fundação para a Ciência e a Tecnologia for Scientific Employment Stimulus Institutional Call (CEECINST/00102/2018) and UIDB/50006/2020 and UIDP/50006/2020 (LAQV), UIDB/00100/2020 and UIDP/00100/2020 (Centro de Química Estrutural).

Data Availability Statement: Data will be made available upon request.

Acknowledgments: The TEM and XEDS analyses were carried out at the Innovation Centre for Nanomaterials and Nanotechnologies of Tomsk Polytechnic University. ICP-AES was performed using the core facilities of TPU’s “Physics and Chemical Methods of Analysis”. XPS analyses were carried out in CEMUP—Center of Materials of the University of Porto, Portugal. S.A.C.C. acknowledges Fundação para a Ciência e a Tecnologia for Scientific Employment Stimulus Institutional Call (DOI 10.54499/CEECINST/00102/2018/CP1567/CT0026) and UIDB/50006/2020 and UIDP/50006/2020 (LAQV), UIDB/00100/2020 and UIDP/00100/2020 (Centro de Química Estrutural).

Conflicts of Interest: The authors declare no conflicts of interest.

References

1. BP. *BP Statistical Review of World Energy 2022*, 71st ed.; BP: London, UK, 2022.
2. British Petroleum. Statistical Review of World Energy Globally Consistent Data on World Energy Markets and Authoritative Publications in the Field of Energy. *BP Energy Outlook* **2021**, *70*, 8–20.
3. Lucas, N.; Kanna, N.R.; Nagpure, A.S.; Kokate, G.; Chilukuri, S. Novel Catalysts for Valorization of Biomass to Value-Added Chemicals and Fuels. *J. Chem. Sci.* **2014**, *126*, 403–413. [[CrossRef](#)]
4. Den, W.; Sharma, V.K.; Lee, M.; Nadadur, G.; Varma, R.S. Lignocellulosic Biomass Transformations via Greener Oxidative Pretreatment Processes: Access to Energy and Value Added Chemicals. *Front. Chem.* **2018**, *6*, 1–23. [[CrossRef](#)]
5. Deng, W.; Feng, Y.; Fu, J.; Guo, H.; Guo, Y.; Han, B.; Jiang, Z.; Kong, L.; Li, C.; Liu, H.; et al. Catalytic Conversion of Lignocellulosic Biomass into Chemicals and Fuels. *Green Energy Environ.* **2023**, *8*, 10–114. [[CrossRef](#)]
6. Jing, Y.; Guo, Y.; Xia, Q.; Liu, X.; Wang, Y. Catalytic Production of Value-Added Chemicals and Liquid Fuels from Lignocellulosic Biomass. *Chem* **2019**, *5*, 2520–2546. [[CrossRef](#)]
7. Hommes, A.; Heeres, H.J.; Yue, J. Catalytic Transformation of Biomass Derivatives to Value-Added Chemicals and Fuels in Continuous Flow Microreactors. *ChemCatChem* **2019**, *11*, 4671–4708. [[CrossRef](#)]
8. Dai, L.; Wang, Y.; Liu, Y.; He, C.; Ruan, R.; Yu, Z.; Jiang, L.; Zeng, Z.; Wu, Q. A Review on Selective Production of Value-Added Chemicals via Catalytic Pyrolysis of Lignocellulosic Biomass. *Sci. Total Environ.* **2020**, *749*, 142386. [[CrossRef](#)]
9. Yang, W.; Du, X.; Liu, W.; Wang, Z.; Dai, H.; Deng, Y. Direct Valorization of Lignocellulosic Biomass into Value-Added Chemicals by Polyoxometalate Catalyzed Oxidation under Mild Conditions. *Ind. Eng. Chem. Res.* **2019**, *58*, 22996–23004. [[CrossRef](#)]
10. Popp, J.; Kovács, S.; Oláh, J.; Divéki, Z.; Balázs, E. Bioeconomy: Biomass and Biomass-Based Energy Supply and Demand. *New Biotechnol.* **2021**, *60*, 76–84. [[CrossRef](#)] [[PubMed](#)]
11. Kannengiesser, J.; Sakaguchi-Söder, K.; Mrukwa, T.; Jager, J.; Schebek, L. Extraction of Medium Chain Fatty Acids from Organic Municipal Waste and Subsequent Production of Bio-Based Fuels. *Waste Manag.* **2016**, *47*, 78–83. [[CrossRef](#)] [[PubMed](#)]
12. Sukiran, M.A.; Loh, S.K.; Abu Bakar, N. Production of Bio-Oil from Fast Pyrolysis of Oil Palm Biomass Using Fluidised Bed Reactor. *J. Energy Technol. Policy* **2016**, *6*, 52–62.
13. de Figueiredo, A.K.; Fernández, M.B.; Nolasco, S.M. High Stearic High Oleic Sunflower Oil Extraction: Influence of Temperature, Moisture, and Dehulling on Kinetic Parameters. *Eur. J. Lipid Sci. Technol.* **2023**, *125*, 2300035. [[CrossRef](#)]
14. Zhang, J.; Guo, Z.; Du, W.; Gu, X.; Wang, M.; Zhang, Z.; Ma, Y.; Chen, G. Preparation and Performance of Vegetable Oils Fatty Acids Hydroxylmethyl Triamides as Crude Oil Flow Improvers. *Pet. Chem.* **2018**, *58*, 1070–1075. [[CrossRef](#)]

15. Köckritz, A.; Blumenstein, M.; Martin, A. Catalytic Cleavage of Methyl Oleate or Oleic Acid. *Eur. J. Lipid Sci. Technol.* **2010**, *112*, 58–63. [CrossRef]
16. Imamura, F.; Fretts, A.; Marklund, M.; Ardisson Korat, A.V.; Yang, W.; Lankinen, M.; Qureshi, W.; Helmer, C.; Chen, T.-A.; Wong, K.; et al. Fatty acid biomarkers of dairy fat consumption and incidence of type 2 diabetes: A pooled analysis of prospective cohort studies. *PLoS Med.* **2018**, *15*, e1002670. [CrossRef]
17. Ello, A.S.; Enferadi-kerenkan, A.; Trokourey, A.; Do, T.O. Sustainable Oxidative Cleavage of Vegetable Oils into Diacids by Organo-Modified Molybdenum Oxide Heterogeneous Catalysts. *J. Am. Oil Chem. Soc.* **2017**, *94*, 1451–1461. [CrossRef]
18. Vassoi, A.; Tabanelli, T.; Sacchetti, A.; Di Gioia, F.; Capuzzi, L.; Cavani, F. The Oxidative Cleavage of 9,10-Dihydroxystearic Triglyceride with Oxygen and Cu Oxide-Based Heterogeneous Catalysts. *ChemSusChem* **2021**, *14*, 2375–2382. [CrossRef]
19. Ciriminna, R.; Fidalgo, A.; Ilharco, L.M.; Pagliaro, M. Herbicides Based on Pelargonic Acid: Herbicides of the Bioeconomy. *Biofuels Bioprod. Biorefining* **2019**, *13*, 1476–1482. [CrossRef]
20. Benessere, V.; Cucciolito, M.E.; De Santis, A.; Di Serio, M.; Esposito, R.; Melchiorre, M.; Nugnes, F.; Paduano, L.; Ruffo, F. A Sustainable Process for the Production of Varnishes Based on Pelargonic Acid Esters. *J. Am. Oil Chem. Soc.* **2019**, *96*, 443–451. [CrossRef]
21. Li, Y. The Application of Caprylic Acid in Downstream Processing of Monoclonal Antibodies. *Protein Expr. Purif.* **2019**, *153*, 92–96. [CrossRef]
22. Suberic Acid. Available online: <https://drugs.ncats.io/drug/6U7Y4M9C1H> (accessed on 30 November 2023).
23. Travaini, R.; Martín-Juárez, J.; Lorenzo-Hernando, A.; Bolado-Rodríguez, S. Ozonolysis: An Advantageous Pretreatment for Lignocellulosic Biomass Revisited. *Bioresour. Technol.* **2016**, *199*, 2–12. [CrossRef]
24. Goyal, R.; Singh, O.; Agrawal, A.; Samanta, C.; Sarkar, B. Advantages and Limitations of Catalytic Oxidation with Hydrogen Peroxide: From Bulk Chemicals to Lab Scale Process. *Catal. Rev. Sci. Eng.* **2022**, *64*, 229–285. [CrossRef]
25. Kulik, A.; Janz, A.; Pohl, M.-M.; Martin, A.; Köckritz, A. Gold-Catalyzed Synthesis of Dicarboxylic and Monocarboxylic Acids. *Eur. J. Lipid Sci. Technol.* **2012**, *114*, 1327–1332. [CrossRef]
26. Santacesaria, E.; Sorrentino, A.; Rainone, F.; Di Serio, M.; Speranza, F. Oxidative Cleavage of the Double Bond of Monoenic Fatty Chains in Two Steps: A New Promising Route to Azelaic Acid and Other Industrial Products. *Ind. Eng. Chem. Res.* **2000**, *39*, 2766–2771. [CrossRef]
27. Nocito, F.; Orlando, I.; Digioia, F.; Aresta, M.; Dibenedetto, A. One-Pot Aerobic Cleavage of Monounsaturated Lipids Catalyzed by Mixed Oxides. *ACS Sustain. Chem. Eng.* **2021**, *9*, 6459–6469. [CrossRef]
28. Nouredini, H.; Kanabur, M. Liquid-Phase Catalytic Oxidation of Unsaturated Fatty Acids. *J. Am. Oil Chem. Soc.* **1999**, *76*, 305–312. [CrossRef]
29. Melchiorre, M.; Benessere, V.; Cucciolito, M.E.; Melchiorre, C.; Ruffo, F.; Esposito, R. Direct and Solvent-Free Oxidative Cleavage of Double Bonds in High-Oleic Vegetable Oils. *Chem. Select* **2020**, *5*, 1396–1400. [CrossRef]
30. Spanring, P.; Prat, I.; Costas, M.; Lutz, M.; Bruijninx, P.C.A.; Weckhuysen, B.M.; Klein Gebbink, R.J.M. Fe(6-Me-PyTACN)-Catalyzed, One-Pot Oxidative Cleavage of Methyl Oleate and Oleic Acid into Carboxylic Acids with H₂O₂ and NaIO₄. *Catal. Sci. Technol.* **2014**, *4*, 708–716. [CrossRef]
31. Dapurkar, S.E.; Kawanami, H.; Yokoyama, T.; Ikushima, Y. Catalytic Oxidation of Oleic Acid in Supercritical Carbon Dioxide Media with Molecular Oxygen. *Top. Catal.* **2009**, *52*, 707–713. [CrossRef]
32. Atapalkar, R.S.; Athawale, P.R.; Srinivasa Reddy, D.; Kulkarni, A.A. Scalable, Sustainable and Catalyst-Free Continuous Flow Ozonolysis of Fatty Acids. *Green Chem.* **2021**, *23*, 2391–2396. [CrossRef]
33. Upadhyay, R.; Rana, R.; Sood, A.; Singh, V.; Kumar, R.; Srivastava, V.C.; Maurya, S.K. Heterogeneous Vanadium-Catalyzed Oxidative Cleavage of Olefins for Sustainable Synthesis of Carboxylic Acids. *Chem. Commun.* **2021**, *57*, 5430–5433. [CrossRef]
34. Guicheret, B.; Da Silva, E.; Philippe, R.; Favre-Reguillon, A.; Vanoye, L.; Blach, P.; Raoul, Y.; De Bellefon, C.; Méta, E.; Lemaire, M. Aerobic Oxidative Cleavage of Vicinal Diol Fatty Esters by a Supported Ruthenium Hydroxide Catalyst. *ACS Sustain. Chem. Eng.* **2020**, *8*, 13167–13175. [CrossRef]
35. Chen, S.; Wu, T.; Zhao, C. Synthesis of Branched Biolubricant Base Oil from Oleic Acid. *ChemSusChem* **2020**, *13*, 5516–5522. [CrossRef]
36. Enferadi-Kerenkan, A.; Ello, A.S.; Do, T.-O. Synthesis, Organo-Functionalization, and Catalytic Properties of Tungsten Oxide Nanoparticles As Heterogeneous Catalyst for Oxidative Cleavage of Oleic Acid As a Model Fatty Acid into Diacids. *Ind. Eng. Chem. Res.* **2017**, *56*, 10639–10647. [CrossRef]
37. Kerenkan, A.E.; Ello, A.S.; Echchahed, B.; Do, T.O. Synthesis of Mesoporous Tungsten Oxide/γ-Alumina and Surfactant-Capped Tungsten Oxide Nanoparticles and Their Catalytic Activities in Oxidative Cleavage of Oleic Acid. *Int. J. Chem. React. Eng.* **2016**, *14*, 899–907. [CrossRef]
38. Gámez, S.; de la Torre, E.; Gaigneaux, E.M. Carbon Supports for the Oxidative Cleavage of Oleic Acid: Influence of Textural Properties. *Mol. Catal.* **2022**, *533*, 112797. [CrossRef]
39. Kolobova, E.; Mäki-Arvela, P.; Grigoreva, A.; Pakrieva, E.; Carabineiro, S.A.C.; Peltonen, J.; Kazantsev, S.; Bogdanchikova, N.; Pestryakov, A.; Murzin, D.Y. Catalytic Oxidative Transformation of Betulin to Its Valuable Oxo-Derivatives over Gold Supported Catalysts: Effect of Support Nature. *Catal. Today* **2021**, *367*, 95–110. [CrossRef]
40. Sharma, S.; Aich, S.; Roy, B. Low Temperature Steam Reforming of Ethanol over Cobalt Doped Bismuth Vanadate [Bi₄(V_{0.90}Co_{0.10})₂O_{11-δ} (BICOVOX)] Catalysts for Hydrogen Production. *J. Phys. Chem. Solids* **2021**, *148*, 109754. [CrossRef]

41. Wang, L.; Li, Q.; Liu, X.; Li, C.; Zhao, Z.; Diao, S.; Cao, D.; Xiang, D.; Wu, C.; Liu, K. Improved CO-PROX Selectivity of CuO/CeO₂ Catalysts by Decorating with Lanthanum via Surface Cu^{ξ+} Redox Site. *Appl. Surf. Sci.* **2024**, *649*, 159087. [[CrossRef](#)]
42. Yang, J.-C.E.; Zhu, M.-P.; Guan, D.; Yuan, B.; Sun, D.D.; Sun, C.; Fu, M.-L. Spin State-Tailored Tetrahedral and Octahedral Cobalt Centers on Millimetric Co-Al Oxide Catalysts as Dual Sites for Synergistic Peroxymonosulfate Activation. *Appl. Catal. B Environ.* **2024**, *342*, 123466. [[CrossRef](#)]
43. Sharma, S.; Yashwanth, P.K.; Roy, B. Deactivation Study of the BICOVOX Catalysts Used in Low Temperature Steam Reforming of Ethanol for H₂ Production. *J. Phys. Chem. Solids* **2021**, *156*, 110138. [[CrossRef](#)]
44. Wang, Y.; Wu, K.; Xu, Y.; Zheng, Y.; Huang, F. Effect of Silica on Generation and Stability of Cu⁺ Cations in CuO/CeO₂ Catalysts for CO Oxidation in H₂-Rich Atmosphere. *Int. J. Hydrogen Energy* **2024**, *53*, 1065–1075. [[CrossRef](#)]
45. Seriyala, A.K.; Chava, R.; Baffoe, J.; Pham, X.T.L.; Leclerc, C.; Appari, S.; Roy, B. Tin and Lanthanum Modified Ni/CeO₂ Catalyst Systems for Low Temperature Steam Reforming of Ethanol. *Int. J. Hydrogen Energy* **2024**, *50*, 239–260. [[CrossRef](#)]
46. Di, M.; Schaefer, A.; Hemmingsson, F.; Bell, T.; Feng, Y.; Skoglundh, M.; Thompsett, D.; Carlsson, P.-A. Why Nitrogen Oxide Inhibits CO Oxidation over Highly Dispersed Platinum Ceria Catalysts. *Catal. Today* **2024**, *426*, 114394. [[CrossRef](#)]
47. Kozhukhova, A.E.; du Preez, S.P.; Bessarabov, D.G. Development of Pt⁻Co/Al₂O₃ Bimetallic Catalyst and Its Evaluation in Catalytic Hydrogen Combustion Reaction. *Int. J. Hydrogen Energy* **2024**, *51*, 1079–1096. [[CrossRef](#)]
48. Pakrieva, E.; Kolobova, E.; Kotolevich, Y.; Pascual, L.; Carabineiro, S.A.C.; Kharlanov, A.N.; Pichugina, D.; Nikitina, N.; German, D.; Partida, T.A.Z.; et al. Effect of Gold Electronic State on the Catalytic Performance of Nano Gold Catalysts in N-Octanol Oxidation. *Nanomaterials* **2020**, *10*, 880. [[CrossRef](#)]
49. Pakrieva, E.; Kolobova, E.; German, D.; Stucchi, M.; Villa, A.; Prati, L.; Carabineiro, S.A.C.; Bogdanchikova, N.; Corberán, V.C.; Pestryakov, A. Glycerol Oxidation over Supported Gold Catalysts: The Combined Effect of Au Particle Size and Basicity of Support. *Processes* **2020**, *8*, 1016. [[CrossRef](#)]
50. German, D.; Pakrieva, E.; Kolobova, E.; Carabineiro, S.A.C.; Stucchi, M.; Villa, A.; Prati, L.; Bogdanchikova, N.; Corberán, V.C.; Pestryakov, A. Oxidation of 5-Hydroxymethylfurfural on Supported Ag, Au, Pd and Bimetallic Pd-Au Catalysts: Effect of the Support. *Catalysts* **2021**, *11*, 115. [[CrossRef](#)]
51. German, D.; Kolobova, E.; Pakrieva, E.; Carabineiro, S.A.C.; Sviridova, E.; Perevezentsev, S.; Alijani, S.; Villa, A.; Prati, L.; Postnikov, P.; et al. The Effect of Sibunit Carbon Surface Modification with Diazonium Tosylate Salts of Pd and Pd-Au Catalysts on Furfural Hydrogenation. *Materials* **2022**, *15*, 4695. [[CrossRef](#)]
52. Kolobova, E.; Kotolevich, Y.; Pakrieva, E.; Mamontov, G.; Farias, M.H.; Bogdanchikova, N.; Corberan, V.C.; Pestryakov, A. Causes of Activation and Deactivation of Modified Nanogold Catalysts during Prolonged Storage and Redox Treatments. *Molecules* **2016**, *21*, 486. [[CrossRef](#)] [[PubMed](#)]
53. Hinojosa-Reyes, M.; Camposeco-Solis, R.; Zanella, R.; Rodríguez-González, V.; Ruiz, F. Gold Nanoparticle: Enhanced CO Oxidation at Low Temperatures by Using Fe-Doped TiO₂ as Support. *Catal. Lett.* **2018**, *148*, 383–396. [[CrossRef](#)]
54. Zanella, R.; Giorgio, S.; Henry, C.R.; Louis, C. Alternative Methods for the Preparation of Gold Nanoparticles Supported on TiO₂. *J. Phys. Chem. B* **2002**, *106*, 7634–7642. [[CrossRef](#)]
55. Zanella, R.; Louis, C. Influence of the Conditions of Thermal Treatments and of Storage on the Size of the Gold Particles in Au/TiO₂ Samples. *Catal. Today* **2005**, *107–108*, 768–777. [[CrossRef](#)]
56. Zanella, R.; Delannoy, L.; Louis, C. Mechanism of Deposition of Gold Precursors onto TiO₂ during the Preparation by Cation Adsorption and Deposition-Precipitation with NaOH and Urea. *Appl. Catal. A Gen.* **2005**, *291*, 62–72. [[CrossRef](#)]
57. Villa, A.; Schiavoni, M.; Campisi, S.; Veith, G.M.; Prati, L. Pd-Modified Au on Carbon as An Effective and Durable Catalyst for the Direct Oxidation of HMF to 2,5-Furandicarboxylic Acid. *ChemSusChem* **2013**, *6*, 609–612. [[CrossRef](#)]
58. Kulik, A.; Martin, A.; Pohl, M.M.; Fischer, C.; Köckritz, A. Insights into Gold-Catalyzed Synthesis of Azelaic Acid. *Green Chem.* **2014**, *16*, 1799–1806. [[CrossRef](#)]
59. Bell, T.E.; González-Carballo, J.M.; Tooze, R.P.; Torrente-Murciano, L. Single-Step Synthesis of Nanostructured γ -Alumina with Solvent Reusability to Maximise Yield and Morphological Purity. *J. Mater. Chem. A* **2015**, *3*, 6196–6201. [[CrossRef](#)]
60. Krishnamurthy, S.; Esterle, A.; Sharma, N.C.; Sahi, S.V. Yucca-Derived Synthesis of Gold Nanomaterial and Their Catalytic Potential. *Nanoscale Res. Lett.* **2014**, *9*, 627. [[CrossRef](#)]
61. John, A.K.; Palaty, S.; Sharma, S.S. Greener Approach towards the Synthesis of Titanium Dioxide Nanostructures with Exposed {001} Facets for Enhanced Visible Light Photodegradation of Organic Pollutants. *J. Mater. Sci. Mater. Electron.* **2020**, *31*, 20868–20882. [[CrossRef](#)]
62. Sayyed, S.A.A.R.; I Beedri, N.; Kadam, V.S.; Pathan, H.M. Rose Bengal-Sensitized Nanocrystalline Ceria Photoanode for Dye-Sensitized Solar Cell Application. *Bull. Mater. Sci.* **2016**, *39*, 1381–1387. [[CrossRef](#)]
63. Kustov, L.M.; Kalenchuk, A.N. Effect of Cr on a Ni-Catalyst Supported on Sibunit in Bicyclohexyl Dehydrogenation in Hydrogen Storage Application. *Catalysts* **2022**, *12*, 1506. [[CrossRef](#)]
64. Molaie, R.; Farhadi, K.; Forough, M.; Hajizadeh, S. Green Biological Fabrication and Characterization of Highly Monodisperse Palladium Nanoparticles Using Pistacia Atlantica Fruit Broth. *J. Nanostructures* **2018**, *8*, 47–54. [[CrossRef](#)]
65. Gualteros, J.A.D.; Garcia, M.A.S.; da Silva, A.G.M.; Rodrigues, T.S.; Cândido, E.G.; e Silva, F.A.; Fonseca, F.C.; Quiroz, J.; de Oliveira, D.C.; de Torresi, S.I.C.; et al. Synthesis of Highly Dispersed Gold Nanoparticles on Al₂O₃, SiO₂, and TiO₂ for the Solvent-Free Oxidation of Benzyl Alcohol under Low Metal Loadings. *J. Mater. Sci.* **2019**, *54*, 238–251. [[CrossRef](#)]

66. Rodrigues, T.S.; Zhao, M.; Yang, T.; Gilroy, K.D.; da Silva, A.G.M.; Camargo, P.H.C.; Xia, Y. Synthesis of Colloidal Metal Nanocrystals: A Comprehensive Review on the Reductants. *Chem. Eur. J.* **2018**, *24*, 16944–16963. [[CrossRef](#)] [[PubMed](#)]
67. Zhu, M.K.; Zhao, J.F.; Loh, T.P. Palladium-Catalyzed C-C Bond Formation of Arylhydrazines with Olefins via Carbon-Nitrogen Bond Cleavage. *Org. Lett.* **2011**, *13*, 6308–6311. [[CrossRef](#)]
68. Yan, X.; Sun, H.; Xiang, H.; Yu, D.G.; Luo, D.; Zhou, X. Palladium-Catalyzed C(carbonyl)-C Bond Cleavage of Amides: A Facile Access to Phenylcarbamate Derivatives with Alcohols. *Chem. Commun.* **2018**, *54*, 8606–8609. [[CrossRef](#)]
69. Nambo, M.; Itami, K. Palladium-Catalyzed Carbon-Carbon Bond Formation and Cleavage of Organo(Hydro)Fullerenes. *Chem. Eur. J.* **2009**, *15*, 4760–4764. [[CrossRef](#)]

Disclaimer/Publisher's Note: The statements, opinions and data contained in all publications are solely those of the individual author(s) and contributor(s) and not of MDPI and/or the editor(s). MDPI and/or the editor(s) disclaim responsibility for any injury to people or property resulting from any ideas, methods, instructions or products referred to in the content.